

Cardiff Behavioral Model of a Ka-Band SPDT Switch Trained on Structured Minimization of Load-Pull Characterization Data

Seyed Urman Ghozati^{§#1}, Ehsan Merhabi Azad[§], Kauser Chaudhry[§], Roberto Quaglia[#], Paul J. Tasker[#]

[§]Compound Semiconductors Applications Catapult, Newport, UK

[#]Cardiff University, Cardiff, UK

¹urman.ghozati@csa.catapult.org.uk

Abstract— This paper demonstrates the Cardiff behavioral model based on the large-signal response of a single pole, double throw switch (SPDT) to realize a tunable reactive termination for advanced power amplifier architectures operating in the Ka-band up to 3 watts. The model was developed using a comprehensive load-pull (LP) characterization dataset comprising 2176 data points. Subsequently, it was trained to replicate this dataset with only 44 input data points, achieving an acceptable accuracy reflected by an NMSE of -33.8 dB.

Keywords— Cardiff model, Behavioral model, SPDT, Ka-band, microwave switches.

I. INTRODUCTION

The Orthogonal Load Modulated Balanced Amplifier (OLMBA) architecture presented by [1], [2] introduces a reactive component, termed “ jX ” at the output isolated port. In the context of an electronically tunable termination, the jX is employed for active load modulation between the main signal and the control signal power (CSP) by fine-tuning the phase and magnitude of the reflected CSP to optimize the performance.

In the design of an OLMBA, one way of realizing the tunable reflective termination is to use a switching network that selects between different reactive components as depicted in Fig. 1. The characteristics of the switching network, including the passive and active components, as well as the loaded reactive component, will determine the final jX termination introduced to the OLMBA. Hence, an extensive understanding of the switching cell and its accompanying passive networks is vital. In literature, the characterization and modeling of the HEMT devices as switching cells operating at various frequencies and non- 50Ω loads, in linear and compressed states, has been investigated [3], [4].

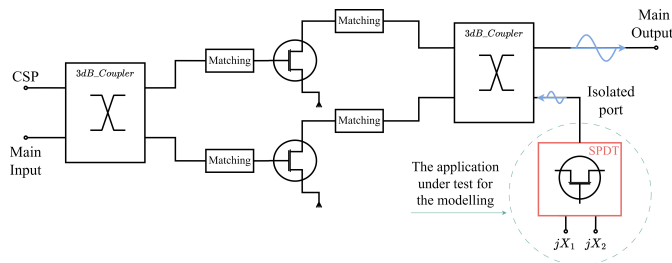
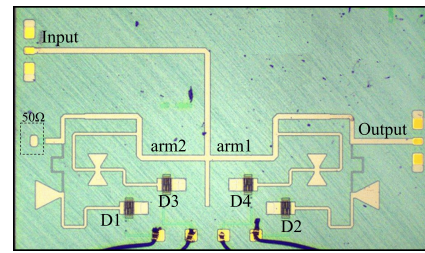


Fig. 1. An OLMBA architecture with output isolated port linked to an SPDT to be introduced to two different reactive components.

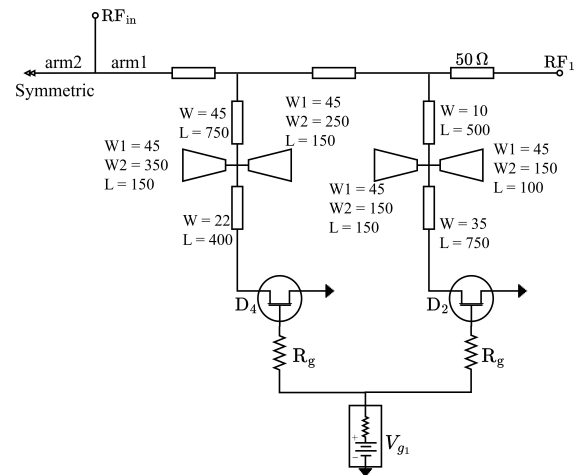
This paper, in the first part, describes a high-power, low-loss Ka-band SPDT designed specifically to realize a tunable reflective termination for OLMBA applications. However, the main focus is on extracting a behavioral model based on LP characterization over input power sweep. The implemented Cardiff behavioral model mathematics and further investigation into its interpolation capabilities on microwave switches demonstrated that a relatively smaller data set during the measurement could also be sufficient to have a model with acceptable accuracy below -30 dB.

II. KA-BAND SPDT SWITCH

Various methodologies can be utilized in the design of SPDT [5], [6]. In this work, a resonating network is designed to compensate for the degradation of the FET-based switching devices at the design frequency.



(a)



(b)

Fig. 2. Microphotograph of the fabricated SPDT (a), the schematic of the same SPDT (only arm1 depicted as it is symmetric design) (b).

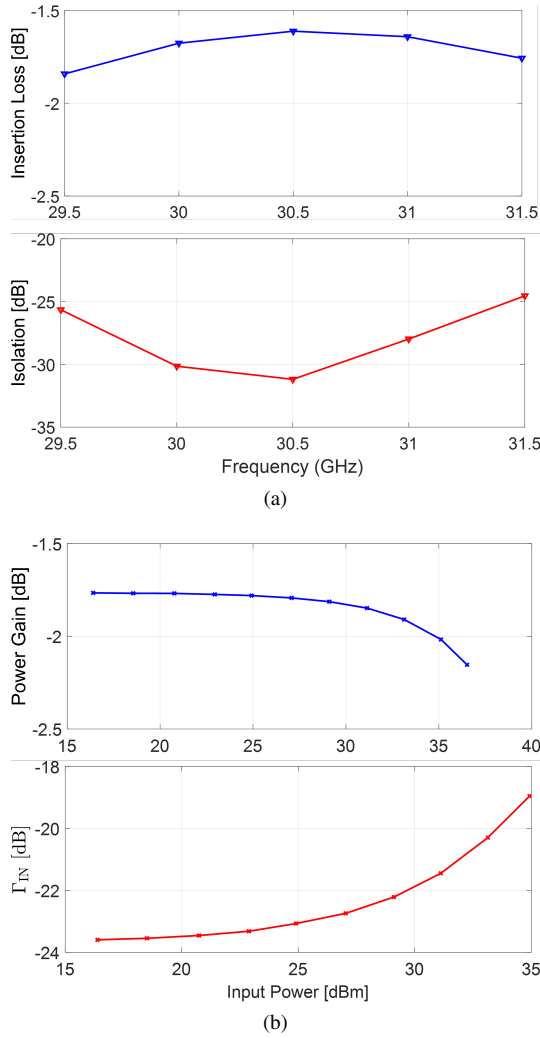


Fig. 3. Characterization of the SPDT in ON and OFF conditions; Small signal measurement results (b), large signal measurement results at 30.5 GHz (c).

The designed SPDT employs the WIN Semiconductors' NP12-01 GaN-on-SiC HEMT structured technology as its switching cells. Due to the absence of a foundry model for the switching cells, these components were initially characterized individually, and the extracted measurement data were subsequently utilized in the SPDT design.

As shown in Fig. 2a, the RF input is a common port for the two outputs that operate complementarily; while one port is active, the other is inactive. The main topology is a reflective shunt design at which the signal entered into the inactive port will be directed to the ground by HEMT devices under ON conditions (low impedance). Such a configuration is expected to enhance low insertion loss behavior. Due to the switching cells' limitation at higher frequencies, especially during the OFF condition, a resonant network is designed preceding the switching cell in parallel branches. Each branch employs two switching cells to enhance the device's isolation characteristics. Fig. 2b depicts the schematic diagram for one arm of the SPDT. Due to the symmetry of the design of the arm1 and arm2, only one arm is depicted in the schematic.

However, each arm has non-symmetrical parallel branches. Fig. 3a and 3b illustrate the SPDT's responses under the small and large signal characterizations. Finally, load-pull characterization with swept input power was performed to extract the necessary data for model development.

III. CARDIFF BEHAVIORAL MODEL

The Cardiff behavioral model, derived from load-pull measurement data at the fundamental frequency, is expressed in the traveling wave domain and incorporates input power dependency as detailed below [7].

$$B_{p,1} = (\angle A_{1,1}) \cdot \sum_x \sum_m \sum_n \dots, \quad K_{p,m,n,x} \cdot |A_{1,1}|^x \cdot |A_{2,1}|^m \cdot \left(\angle \frac{A_{2,1}}{A_{1,1}} \right)^n \quad (1)$$

While the interpolation capabilities of the Cardiff model have been explored previously [4], the extent of these capabilities and their potential to reduce reliance on extensive datasets during measurements have not been investigated in microwave switches. Equation 1 highlights the direct influence of the input components A_{11} and A_{21} . Hence, the impact of the reduced number of A_{21} and A_{11} for a truncated 5th order model became our main focus during the modeling of the SPDT.

The reduction in data points was initiated through the random selection of the phase and magnitude of the input components (A_{21} and A_{11}), maintaining consistent indexing to form different numbers of reflection coefficients while incorporating all 16 power levels. It is important to note that, at this stage, the correlation between the selected data points of the input components (A_{21} and A_{11}) and the corresponding reflection coefficient (Γ) locations on the Smith chart was not considered. The Fig. 4 illustrates the model's accuracy, represented by the corresponding NMSE of the B_{21} component, based on the reduced number of input components, provide insight into the lower limits for dataset reduction, establishing 11 load points as a basis for further investigation.

The reduction of power levels was incorporated as an additional variable to further minimize the input components

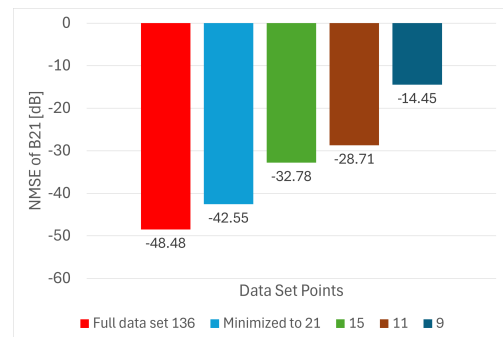


Fig. 4. Accuracy comparison of modeled B_{21} variable demonstrated by NMSE parameter over the full data set (red) and minimized data sets of: 21 points (blue), 15 points (green), 11 points (brown) and 9 points (navy).

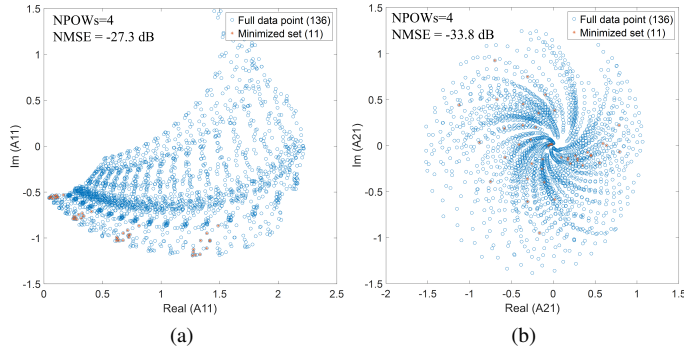


Fig. 5. NMSE dependency on input components incorporating 4 power levels; not-distributed A_{11} component (a), selectively distributed A_{21} component (b).

while monitoring the resulting NMSE. Fig. 5a illustrates the use of A_{11} to represent the reduced power levels, their arrangement, and the corresponding extracted NMSE.

Upon observing A_{21} with the same arrangement previously applied, it was realized that the random phase selection did not necessarily span the entire dataset. Consequently, the data points were selectively chosen to ensure broader coverage across the data sets lead to an NMSE improvement from -27 dB in Fig. 5a to -33 dB in Fig. 5b.

It is important to note that the applied random selection worked experimentally in this case, but there is not enough data to predict if it would work in general on other switches or other DUTs. For amplifier transistors, selection methods of “A” patterns have been proven [8]. However, those methods were not used in our work as they require setting the waves, which is not possible with the passive load-pull system available. Moreover, While modeling time savings were not quantified directly, the reduced number of measurement points significantly contributes to actual time savings during the measurement phase.

Satisfied with the extracted enhanced NMSE, the final model was extended within the same environment to include the input and output reflection coefficients (Γ_{in} and Γ_L) as the primary parameters for the tunable reflective termination application. Fig. 6 illustrates the measured data for the full data set (136 loads at 16 power levels) depicted in red squares. The localized model is derived from a minimized data set of 44 points, consisting of 11 loads across 4 power levels shown with black squares. The trained model, represented by blue squares, is based on the same 44-point data set but interpolates to 136 loads at 16 power levels, replicating a total of 2176 data points within the extraction domain.

The selectively distributed phase of the A_{21} and A_{11} components led to more diverse reflection coefficients (Γ) across the Smith chart, as represented by the black squares in Fig. 6a and Fig. 6b. Additionally, the corresponding model points (blue squares) exhibit reduced error compared to the random selection approach which validates the enhanced NMSE from -27 dB to -33 dB. This highlights a critical insight: defining measurement loads in advance to cover different regions of the Smith chart, even with a reduced dataset, can

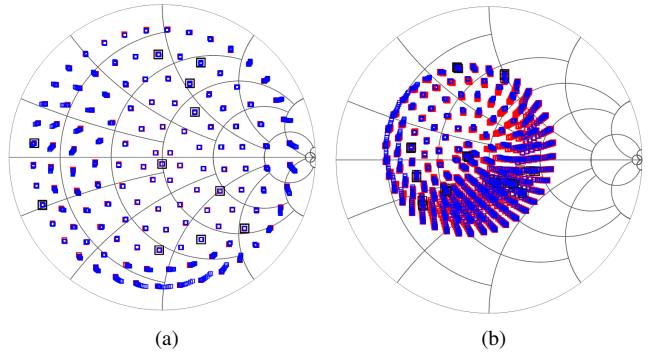


Fig. 6. Comparison of the measured data set (red) versus localized model (black) and trained model (blue); output reflection coefficients (Γ_L) (a), input reflection coefficients (Γ_{IN}) (b).

yield a model with comparable accuracy. Such an approach significantly improves the process by reducing measurement time, cost, and post-processing requirements.

In Fig. 6a, the measured data exhibit small deviations, particularly near the boundaries where $|\Gamma| = 1$, likely attributable to measurement system limitations. On the other hand, Fig. 6b reveals a convergence-like behavior of Γ_{in} toward its own center on the Smith chart. This tendency can be associated with the inherent losses of the switching cells and SPDT’s passive networks. Additionally, Γ_{in} displays a consistent shift toward the short-circuit point, which may be influenced by the electrical length of the trace connecting the common point to the RF input pad. This behavior suggests that the trace length exerts a notable reactive impact on the impedance transformation within the switch.

In the context of the tunable reflective termination, it is important to note that the common RF input will always interact with the jX of the active output of the SPDT. Consequently, modeling the inactive output is unnecessary as long as its isolation remains sufficient. Therefore, the modeling of inactive output is not addressed in Fig. 6a. Accordingly, the analysis of the power gain variable was conducted exclusively at the active output by comparing the measured data with both the localized model and the trained model at 50Ω , as depicted in Fig. 7.

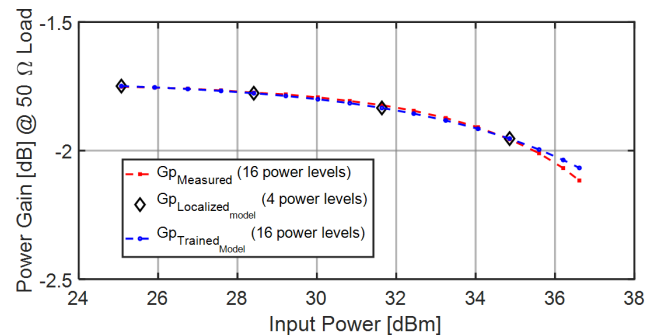


Fig. 7. Comparison of measured power gain (red) from the SPDT in its active mode at the $\Gamma_L = 50 \Omega$ with the corresponding values predicted by the localized model (black) and the trained model (blue).

IV. CONCLUSION

The behavioral model of a fabricated Ka-band SPDT switch, designed to handle power levels up to 3 Watts, has been effectively trained using a substantially minimized dataset. The resulting model demonstrates high accuracy, achieving an NMSE of -33.8dB while utilizing only 11 distinct load conditions across four power levels. This corresponds to 2% of the original measurement dataset and enables interpolation to a dataset comprising 2176 points. This can be attributed to the fact that the operation of interest for the SPDT switch occurs under linear conditions, which likely facilitates more accurate predictions in the behavioral model.

In future work, this approach could be applied during the measurement process to enhance efficiency by fewer data point to measure and support further model feature development, such as extrapolation.

ACKNOWLEDGMENT

The authors would like to express their gratitude to WIN Semiconductors for fabricating the SPDT.

REFERENCES

- [1] D. J. Collins, R. Quaglia, J. R. Powell, and S. C. Cripps, "The orthogonal Imba: A novel rfa architecture with broadband reconfigurability," *IEEE Microwave and Wireless Components Letters*, vol. 30, no. 9, pp. 888–891, 2020.
- [2] J.-B. Urvoy, R. Quaglia, J. R. Powell, and S. C. Cripps, "Experimental characterization of a dual-input olmba for back-off efficiency improvement," in *2023 53rd European Microwave Conference (EuMC)*, 2023, pp. 267–270.
- [3] S. U. Ghazati, A. Baddeley, and R. Quaglia, "Large-signal characterization and behavioral modeling of mm-wave gan hemt switches tailored for advanced power amplifier architectures," in *2024 IEEE Topical Conference on RF/Microwave Power Amplifiers for Radio and Wireless Applications (PAWR)*, 2024, pp. 21–23.
- [4] S. U. Ghazati, R. Quaglia, E. Azad, J. Powell, P. Tasker, and S. Cripps, "Load pull-driven behavioral modelling of microwave switches for the design of tunable reflective terminations," in *2023 18th European Microwave Integrated Circuits Conference (EuMIC)*, 2023, pp. 1–4.
- [5] W. McLevige and V. Sokolov, "Resonated GaAs FET devices for microwave switching," *IEEE Transactions on Electron Devices*, vol. 28, no. 2, pp. 198–204, 1981.
- [6] Y. Tajima, W. Titus, R. Mozzi, and A. Morris, "Broadband GaAs FET 2×1 switches," in *1984 IEEE GaAs IC Symposium Technical Digest*, 1984, pp. 081–084.
- [7] P. J. Tasker and J. Benedikt, "Waveform inspired models and the harmonic balance emulator," *IEEE Microwave Magazine*, vol. 12, no. 2, pp. 38–54, 2011.
- [8] M. Tian, J. J. Bell, R. Quaglia, E. M. Azad, and P. J. Tasker, "Artificial neural network nonlinear transistor behavioral models: Structure and parameter determination process based on the cardiff model," *IEEE Transactions on Microwave Theory and Techniques*, vol. 73, no. 2, pp. 745–759, 2025.